INTERNATIONAL JOURNAL FOR NUMERICAL METHODS IN FLUIDS, VOL. 22, 815–834 (1996)

VERTICAL DISCRETIZATION IN TIDAL FLOW SIMULATIONS

ANDRÉ B. FORTUNATO AND ANTÓNIO M. BAPTISTA

Center for Coastal and Land-Margin Research and Department of Environmental Science and Engineering, Oregon Graduate Institute of Science & Technology, PO Box 91000, Portland, OR 97291-1000, U.S.A.

SUMMARY

We propose an empirical law for vertical nodal placement in tidal simulations that depends on a single parameter p. The influence of dimensionless numbers on the optimal value of p is analysed through a series of numerical experiments for an individual vertical and a single value of p is found to be adequate for all cases. The proposed law can lead to gains in accuracy of over two orders of magnitude relative to a uniform grid and compares favourably with non-uniform grids previously used in the literature. In practical applications the most effective use of this law may require each vertical to have a different number of nodes. Criteria for the distribution of the total number of nodes among different verticals are also proposed, based on the concept of equalizing errors across the domain. The usefulness of the overall approach is demonstrated through a two-dimensional laterally averaged application to a synthetic estuary.

KEY WORDS: vertical discretization; sigma co-ordinates; localized sigma co-ordinates; tidal flow; numerical experimentation

1. INTRODUCTION

Two general approaches have been used for the horizontal discretization of the flow and transport equations in estuarine and coastal models: unstructured (typically finite elements) and structured (primarily finite differences) grids. While finite elements allow for far superior flexibility in the description of irregular boundaries and in the placement of local refinements, finite difference grids lead to simpler and arguably more efficient (in a node-per-node basis) algorithms.

By contrast, structured grids have been the norm for vertical discretization. Methods using both orthogonal[1,2] (z-co-ordinate) and curvilinear[3–5] (sigma co-ordinate) grids have been extensively used. Sigma co-ordinates are probably the most popular (see review by Cheng and Smith[6]), offering three main advantages relative to z-co-ordinates: (a) a better resolution of shallow areas; (b) a smooth representation of the bottom topography; (c) a simpler treatment of the free surface. The major disadvantage associated with sigma co-ordinates is the potential for generation of large errors in the evaluation of horizontal gradients near steep slopes.[7–9] However, several techniques can be used to reduce these errors considerably.[10–12] Moreover, z-co-ordinate models can also suffer from similar problems.[13]

Recently we proposed what can be seen as the loose vertical equivalent to horizontal unstructured grids.[14] Denoted *localized sigma co-ordinates* (LSCs), this approach combines the main advantages, as well as disadvantages, of traditional *domain-wide sigma co-ordinates* (DWSCs) with a higher

CCC 0271–2091/96/090815–20

Received 16 December 1994
Revised 15 June 1995

flexibility to discretize the vertical direction: the nodal placement is independent for each vertical, so local refinements do not carry over to the rest of the domain.

The concept behind LSCs is simple. As in DWSCs, the height of the water column is linearly mapped into a fixed interval. However, LSCs recognize the solution of the internal mode as an essentially one-dimensional *localized problem* rather than dividing the domain into levels. Therefore each vertical is discretized independently from the others. Horizontal gradients of depth-dependent quantities, which constitute the only direct link between nodes in adjacent verticals, can be computed in either Cartesian or sigma co-ordinates by interpolating the necessary quantities at neighbouring verticals.[13–16] Interpolations increase slightly the computational costs[14] and may make LSCs more awkward to implement on some computer architectures. In the examples presented in this paper, these interpolations are avoided by considering only barotropic flows and neglecting advection and horizontal diffusion.

The use of unstructured grids in the vertical direction can lead to important computational savings relative to the methods currently used. For instance, stratified areas require a fine local discretization[17] which cannot be achieved efficiently using structured grids. Also, one of the trends in ocean modelling is to simulate increasingly larger domains, including simultaneously both deep ocean areas and shallow coastal seas.[18] Clearly, different areas will typically require a different vertical resolution. In deep areas, friction is unimportant and a coarse resolution is sufficient near the bottom as long as a slip bottom boundary condition is used; in contrast, a good representation of the bottom boundary layer is needed in shallow areas.

Still, one cannot take full advantage of the flexibility of LSCs without appropriate criteria to discretize the vertical dimension. The primary purpose of this paper is to develop a criterion for vertical nodal placement. Because a very large number of parameters can potentially influence an optimal discretization, this study is restricted to unstratified tidal flows. In spite of the relative simplicity of these flows, the criterion proposed herein can greatly reduce the errors in tidal simulations relative to vertically uniform grids and provide useful guidelines for the simulation of more complex flows.

The criterion developed here addresses both the nodal distribution in a single vertical and the horizontal distribution of the total number of nodes among different verticals. This criterion can be applied on three different levels of complexity. While the two more complex forms lead to a varying number of nodes per vertical (thus requiring the use of LSCs), the simplest form can also be applied to DWSC models.

Previous work on vertical discretization strategies is surprisingly scarce. Noye[19] proposed the use of a 'kappa grid' which allows a higher resolution near the bottom. Errors relative to a uniform grid are significantly reduced while maintaining second-order accuracy in $\Delta\sigma$.[20] However, optimal kappa grids vary strongly with frictional parameters, making the method difficult to use in practice. Davies[21] compared four approaches to discretize the vertical (a kappa grid, logarithmic and log–linear grids, and a spectral method) and found that the spectral method and the log–linear grid provide the fastest convergence. However, either one or two parameters need to be specified in all four of these methods and no criteria for their specification were proposed. The method presented herein compares favourably with the logarithmic and log–linear grids.

This paper includes five sections in addition to the introduction. Section 2 describes the model used in the numerical tests and introduces the relevant dimensionless numbers. Section 3 introduces two types of grids and establishes the optimal distribution of the nodes in a single vertical based on the effect of the dimensionless numbers. Section 4 addresses the distribution of the total number of nodes among the different verticals. Section 5 presents an application to a two-dimensional, laterally averaged synthetic estuary to illustrate the gains in accuracy achieved with the optimized grids. Finally, Section 6 presents a summary and some concluding remarks.

2. NUMERICAL FORMULATION AND DIMENSIONLESS NUMBERS

The propagation of tides is generally modelled with the shallow water equations, which describe the conservation of mass and momentum under the conventional hydrostatic pressure and Boussinesq approximations. Here we further neglect advective accelerations and rotation effects in order to decouple the two horizontal momentum equations. Advective accelerations can be neglected because they are usually small compared with the gravity term, while rotation was shown to have little effect on the convergence of several numerical methods to solve the vertical structure of tidal flows.[21] With these simplifications each momentum equation can be written as

$$\frac{\partial u}{\partial t} = -g\frac{\partial \eta}{\partial x} + \frac{\partial}{\partial z}\left(A_v \frac{\partial u}{\partial z}\right), \tag{1}$$

where x and z are the Cartesian co-ordinates, t is time, u is the horizontal velocity, η is the elevation of the water surface, g is the gravitational acceleration and A_v is the vertical eddy viscosity.

Most three-dimensional shallow water numerical models decouple the treatment of the horizontal and vertical dimension in an explicit recognition of the different space and time scales involved. The decoupling is usually accomplished by the introduction of external and internal modes. Loosely stated, the external mode determines the elevations (and in some cases the depth-averaged velocities) while the internal mode resolves the vertical structure of the flow.

Consistent with the objectives of this paper, we will concentrate here on the internal mode. To isolate this model, we assume an elevation field of the form

$$\eta = A\cos\left(\frac{2\pi t}{T} + \phi\right), \tag{2}$$

where A, T and ϕ are the wave amplitude, period and phase respectively. The gravity forcing can then be written as

$$g\frac{\partial \eta}{\partial x} = g\frac{\partial A}{\partial x}\cos\left(\frac{2\pi t}{T} + \phi\right) - gA\frac{\partial \phi}{\partial x}\sin\left(\frac{2\pi t}{T} + \phi\right) \tag{3}$$

or, after rearrangement,

$$g\frac{\partial \eta}{\partial x} = -\frac{2\pi U}{T}\cos\left(\frac{2\pi t}{T} + \phi + \phi'\right), \tag{4}$$

where we introduce a freestream velocity U and a phase ϕ' defined as

$$U = \frac{gT}{2\pi}\sqrt{\left[\left(\frac{\partial A}{\partial x}\right)^2 + \left(A\frac{\partial \phi}{\partial x}\right)^2\right]}, \tag{5}$$

$$\phi' = \tan^{-1}\left(A\frac{\partial \phi}{\partial x}\Big/\frac{\partial A}{\partial x}\right). \tag{6}$$

Physically, the freestream velocity represents the velocity amplitude in the absence of friction. In deep waters, where the effect of dissipation is restricted to the bottom layer, U represents closely the actual velocity amplitude near the surface.

Equation (1) is solved assuming zero stress at the surface and using a quadratic bottom slip condition:

$$\left.\frac{\partial u}{\partial z}\right|_{z=0} = 0, \qquad \left.\frac{\partial u}{\partial z}\right|_{z=-h} = c_d|u_b|u_b. \tag{7}$$

Here c_d is a dimensionless friction coefficient, h is the depth and the subscript 'b' represents values at the bottom. A rigid-lid approximation is used for simplicity.

In order to reduce the number of physical parameters involved, (1) and (7) are written in dimensionless form. Dimensionless quantities are defined as

$$v = u/U, \qquad \tau = t/T, \qquad \sigma = z/h, \qquad E = A_v/hU, \qquad \Gamma = UT/h. \tag{8}$$

The momentum equation becomes

$$\frac{\partial v}{\partial \tau} = 2\pi \cos(2\pi\tau + \phi + \phi') + \Gamma \frac{\partial}{\partial \sigma}\left(E \frac{\partial v}{\partial \sigma}\right) \tag{9}$$

and the boundary conditions become

$$\left.\frac{\partial v}{\partial \sigma}\right|_{\sigma=0} = 0, \qquad \left. E_b \frac{\partial v}{\partial \sigma}\right|_{\sigma=-1} = c_d |v_b| v_b. \tag{10}$$

Examination of the above equations suggests that three dimensionless numbers determine the behaviour of the solution: Γ, c_d and E. While Γ and c_d are relatively simple to determine, E can vary both in time and along the vertical. For simplicity, E is assumed to be time-independent, an assumption that will be relaxed later. Furthermore, a simple (yet realistic) vertical profile is used to keep the number of parameters to a minimum:

$$E = \begin{cases} E_b + (1+\sigma)(E_c - E_b)/0{\cdot}2, & -1 \leqslant \sigma \leqslant -0{\cdot}8, \\ E_c, & -0{\cdot}8 \leqslant \sigma \leqslant 0, \end{cases} \tag{11}$$

where E_b and E_c represent the dimensionless eddy viscosities at the bottom and in the bulk of the water column respectively. This form of eddy viscosity profile is supported by observations[22] and has been used by a number of modellers.[5,23]

The numerical solution of (9) and (10) forms the basis of our vertical model. The momentum equation is discretized in space with linear finite elements. All terms are centred in time except the viscosity term, which is treated implicitly for stability.

3. NODAL DISTRIBUTION IN A SINGLE VERTICAL

The optimization of the nodal distribution for a single vertical is accomplished in four steps. First we define physically relevant ranges for the dimensionless numbers introduced in the previous section (Γ, c_d, E_b and E_c). Then we select a general expression for nodal placement, controlled by a single parameter p for simplicity. Next, several experiments are carried out to study the effect of each dimensionless number on the optimal value of p. Finally the results from the optimal grid are compared against those obtained with previously proposed vertical discretizations.[21]

3.1. Dimensionless numbers

The freestream velocity scales as $U \propto A\sqrt{(g/h)}$ (equation (5)) and Γ can be scaled as $\Gamma \propto AT\sqrt{(g/h^3)}$. Assuming ranges of T, h and A of 10^4–10^5 s, 1–1000 m and 0·1–10 m respectively, Γ varies between 10^{-1} and 10^5. (The combination $A = 10$ m, $h = 1$ m was not considered realistic.) Values of the friction coefficient c_d used in the literature vary between 0·0025 (minimum recommended by Blumberg and Mellor[3]) and 0·05 (as an extreme case, Walters[5] uses up to 0·07 in Delaware Bay). The dimensionless bottom eddy viscosity scales as $E_b \propto \kappa z_0 \sqrt{(|\tau_b|\rho)}/hU \propto \kappa z_0 \sqrt{c_f}/h$, where κ is the von Kármán constant, z_0 is the roughness length, τ_b is the bottom friction and c_f is a dimensionless friction coefficient for depth-averaged models. Using values of z_0 between 0·001 and 0·1 m and values of c_f between 10^{-3} and 5×10^{-3} suggests a range of E_b between 10^{-8} and 10^{-3}. Finally, Davies and Aldridge[24] suggest $E_c = 0{\cdot}0025\bar{u}/U$, where u represents the depth-averaged velocity. We will therefore take E_c between 10^{-3} and 10^{-2}.

3.2. *Vertical grids*

Two expressions for nodal placement which allow a finer grid spacing near the bottom are studied. The first expression ('grid α') was originally proposed for baroclinic flows:[8]

$$\sigma_i = -\left(\frac{i-n}{1-n}\right)^p, \quad i = 1, \ldots, n, \tag{12}$$

where n is the number of nodes and p determines the degree of near-bottom resolution. A uniform grid in the σ-domain corresponds to $p = 1$ and decreasing (increasing) values of p lead to increasingly finer grids near the bottom (surface). The second expression ('grid β') is given by

$$\sigma_i = \left(\frac{1-i}{1-n}\right)^{1/p} - 1, \quad i = 1, \ldots, n. \tag{13}$$

Grid β represents an adjustment introduced in this work to better reflect the physics of tidal flows. The variation in vertical profiles of velocity in tidal flows is very rapid near the bottom and decreases upwards. In order to obtain accurate results efficiently, the vertical grid spacing should vary in a similar manner. As a first-order approximation the vertical grid spacing is given by the derivatives of the continuous forms of (12) and (13) for α and β respectively:

$$a'(x) = \frac{p}{n-1}\left(\frac{x-n}{1-n}\right)^{p-1}, \qquad b'(x) = \frac{1}{p}\left(\frac{1-x}{1-n}\right)^{1/p-1}, \tag{14}$$

where $x \in [1, n]$ and $p \in]0, 1[$. The function b' is parabolic and can therefore represent a typical velocity profile much better than a' which is hyperbolic.

The difference between grids α and β is illustrated in Figure 1. In grid α the reduction in spatial resolution near the bottom is slower than the corresponding increase in resolution near the surface, while the reverse occurs with formulation β. As a result, properly resolving the bottom layer with grid α can lead to too coarse a resolution near the surface, a problem that grid β avoids. Relative to the logarithmic and log-linear grids proposed by Davies,[21] both the α and β grids have two convenient advantages: they include the uniform grid as a particular case and the first node ($i = 1$) is naturally placed at the bottom. Although the log–linear and β grids appear very similar on the scale shown in Figure 1, the β grid is somewhat coarser near the bottom.

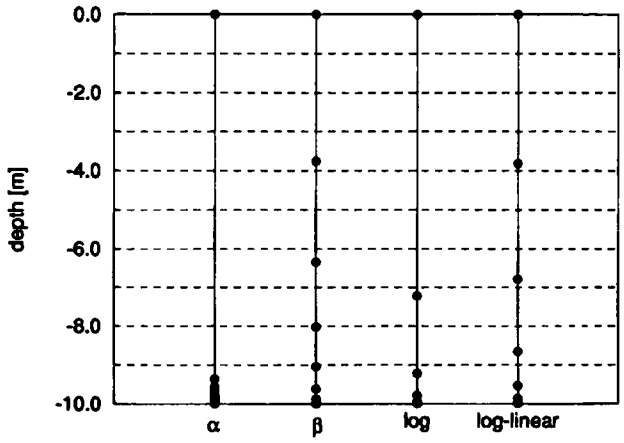

Figure 1. Examples of 10-node α ($p = 0{\cdot}03$) and β ($p = 0{\cdot}25$) grids for 10 m depth. Logarithmic and log–linear grids[21] are also included for comparison

The performance of grids α and β is compared using the default values of the dimensionless numbers (Table I). A dimensionless time step of 10^{-3} is used in all simulations. The model is run for 10 tidal cycles and the time series of velocity at each node from the last cycle are harmonically analysed to extract the amplitudes and phases of the two relevant dimensionless frequencies F_1 (the forcing frequency) and F_3 (the third harmonic, generated by non-linear friction). Results are compared with those obtained using a very fine reference grid with 10^4 nodes and a time step of 10^{-4}. We chose a β grid with $p=0{\cdot}6$ as reference, because uniform grids did not provide enough resolution near the bottom even for as many as 10^4 nodes. The accuracy of the reference grid was verified by running one of the tests with a 10^5-node grid and comparing the results. L_2-norms of amplitudes and phases are computed for each frequency as

$$L_2(\theta_r) = \sqrt{\left(\int_{-1}^{0} (\theta_r - \tilde{\theta}_r)^2 \mathrm{d}\sigma\right)}, \tag{15}$$

where θ represents a generic variable, the subscript r represents either amplitudes or phases and the tilde stands for the reference solution. Note that only relative amplitude errors can be computed, since U is not known.

Amplitude and phase errors for Test 1 are shown in Figure 2 as a function of p for both grid types. Grid β is much better than grid α: not only is the optimal value of p, p_{opt}, only weakly dependent on the number of nodes, but errors are much smaller. The weak dependence of p_{opt} on the number of nodes will prove very convenient to establish criteria for node placement. Because of the need to resolve the bottom layer properly, p_{opt} for the α grid tends to be very small, resulting in grids that are much too coarse in most of the water column (e.g. $n=30$ and $p=0{\cdot}05$ lead to $\Delta\sigma=0{\cdot}845$ at the surface). This is similar to the behaviour reported by Davies[21] for the kappa grid and explains the poorer accuracy relative to β grids. Grid α is therefore abandoned hereafter.

Test 1 illustrates the importance of using non-uniform grids. Not only are the errors with regular grids very large ($p=1$ in Figure 2), but the convergence of the solutions is slow relative to an optimized β grid. In particular, insufficient resolution near the bottom can lead to a serious underprediction of velocities in the entire water column (Figure 3).

The results for the β grid (Figure 2) also suggest that p_{opt} is the same for both F_1 and F_3 and for both amplitudes and phases. We will take advantage of these two properties in the discussion of the remaining 1D tests, where we will only show results for the amplitudes of the primary constituents.

We note, however, that the independence of p_{opt} from the frequency does not necessarily extend to more complex conditions, including higher dimensions. Indeed, we believe that this independence results in our 1D tests from two reasons. First, F_3 is generated by F_1, so errors in the primary constituent will be reflected in the overtides. Secondly, profiles for both F_1 and F_3 have very large

Table I. Parameters used in tests 1–5. Default values are shown in bold

Test	Γ	c_d	E_b	E_c
1	**10^4**	**0·005**	**10^{-5}**	**0·0025**
2	10^{-1}, 10^0, 10^1 10^2, 10^3, **10^4**, 10^5	**0·005**	**10^{-5}**	**0·0025**
3	**10^4**	0·0225, **0·005**, 0·001, 0·05	**10^{-5}**	**0·0025**
4	**10^4**	**0·005**	10^{-8}, 10^{-7}, 10^{-6}, **10^{-5}**, 10^{-4}, 10^{-3}	**0·0025**
5	**10^4**	**0·005**	**10^{-5}**	0·001, **0·0025**, 0·01

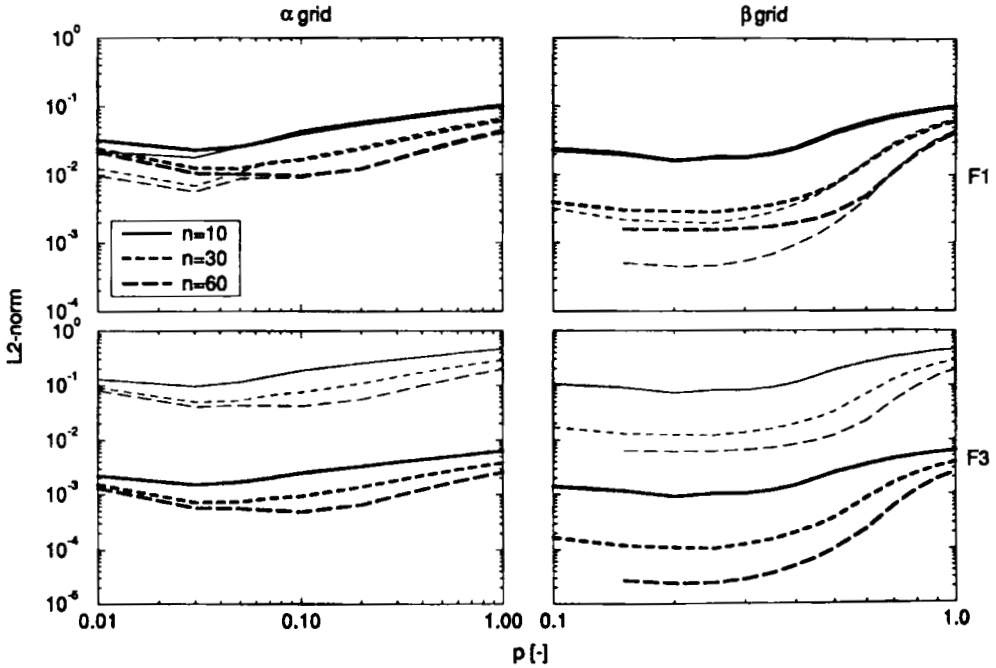

Figure 2. Test 1. L_2-norms of velocities for α and β grids. Thick lines, amplitudes (dimensionless); thin lines, phases (radians)

gradients near the bottom, although for different reasons: the primary constituent decreases sharply near this boundary owing to friction, while the non-linear constituent is generated at the bottom and diffuses slowly upwards. In more realistic simulations, F_3 may have smaller gradients near the bottom, both because it can be forced directly by gravity and because it is also generated in the water column by the interaction between velocity and time-dependent eddy viscosity.[25] Under these circumstances, p_{opt} may depend more strongly on the specific constituent than implied by our tests.

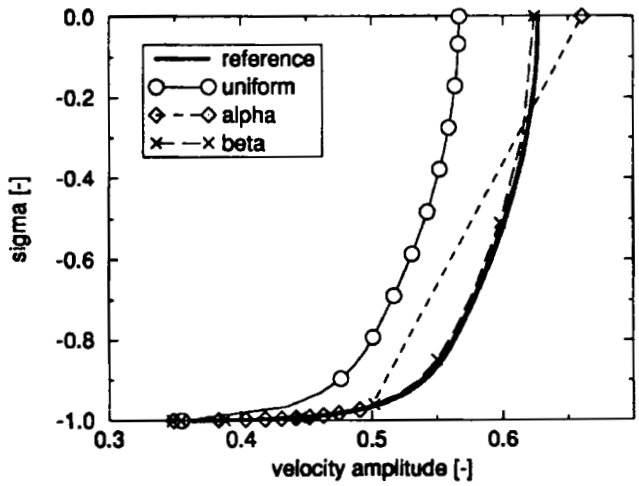

Figure 3. Test 1. Profiles of F_1 velocity amplitude obtained with different 30-node grids. The α and β grids are the optimal for this test (p equals 0·05 and 0·25 respectively)

3.3. *Optimization*

Tests 2–5 examine the effect of the dimensionless numbers Γ, c_d, E_b and E_c on p_{opt}. In each test case a number is varied while the others are held constant (Table I). The vertical profiles of the F_1 amplitude (Figure 4) suggest that the various dimensionless numbers have very different effects on p_{opt}.

1. As Γ increases, the bottom boundary layer includes a growing portion of the water column, which should increase p_{opt}. Still, significant shear remains near the bottom even for the larger values of Γ, so p_{opt} should remain small.
2. The friction coefficient c_d controls the magnitude of the velocities but has very little effect on the shape of the velocity profile and therefore should not affect p_{opt} significantly.
3. Increasing E_b has two effects. First, it reduces velocities just like decreasing c_d does (see equation (10)). Secondly, it reduces shear at the bottom by making the eddy viscosity more uniform over depth. This second effect will make p_{opt} increase with E_b, as fewer nodes will be needed to resolve the bottom layer.
4. Reducing E_c also leads to a more uniform eddy viscosity and thus to a larger p_{opt}.

This qualitative analysis is supported by the results of numerical experimentation. Indeed, concentrating on the variation in the L_2-norms of velocity amplitudes with p, we observe the following.

1. When Γ increases, p_{opt} rises very mildly (Figure 5). Still, the error curves are almost flat in a large region around p_{opt} (around 0·15–0·3), so the effect of Γ on p_{opt} is secondary. The major consequence of increasing Γ is the error growth: the minimum L_2-norm grows by about two orders of magnitude when Γ goes from 10^{-1} to 10^4. For $\Gamma = 10^5$ the errors decrease, possibly

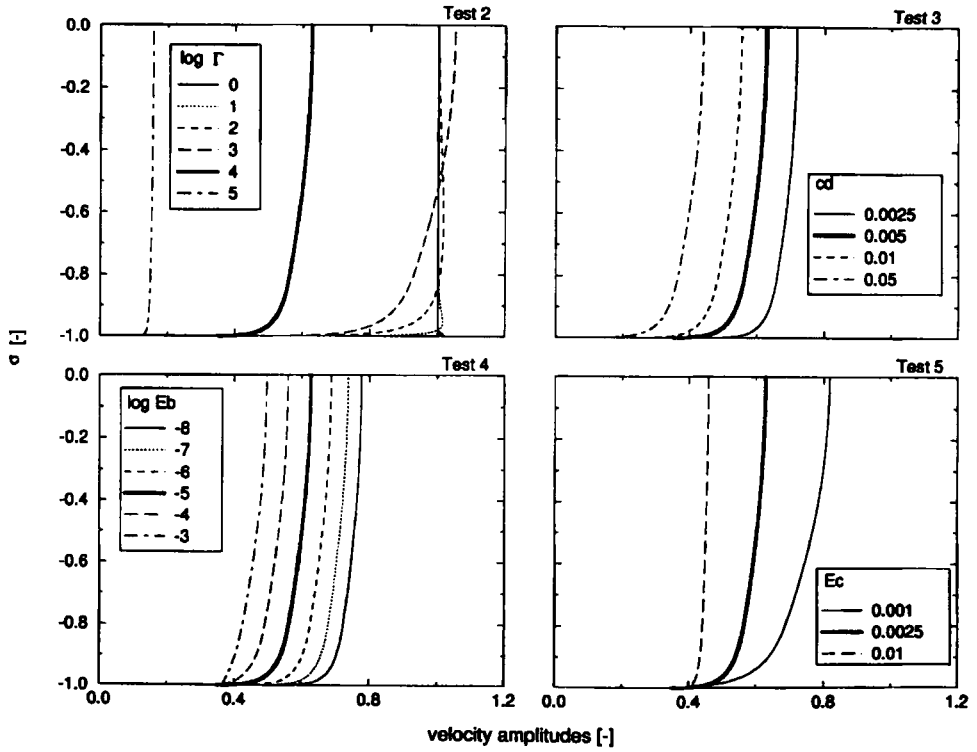

Figure 4. Tests 2–5. Velocity amplitudes (reference simulations)

because friction becomes a dominant process and the dimensionless velocities decrease by almost an order of magnitude (Figure 4).

2. The effect of c_d on the errors is very mild (Figure 6). The L_2-norms decrease slightly with c_d owing to the reduction in the velocity, but p_{opt} remains unchanged.
3. The bottom dimensionless eddy viscosity has a dramatic impact on the L_2-norm behaviour (Figure 7), just as it had on the velocity profiles. The value of p_{opt} tends to increase with E_b owing to a reduction in shear. However, the main effect of the loss of vertical structure of the flow is the flattening of the L_2-norm curves. As an example, for $E_b = 10^{-3}$ and $n = 30$ the difference between the maximum and minimum L_2-norms is less than 20 per cent. Therefore using a small value of p for large E_b will not affect the errors significantly.
4. E_c has only a minor effect on the error curves, perhaps owing to the small range of variation in this number (Figure 8). Again these curves tend to flatten as E_c approaches E_b, but p_{opt} remains mostly unchanged.

In general, tests 2–5 suggest that a single value of p_{opt} (around 0·2–0·3) may be retained. Even though it seems possible to determine a relationship between p_{opt} and the four dimensionless numbers using some kind of optimization technique, eventual gains in accuracy should be marginal. Furthermore, in practical applications with complex turbulence models the determination of E_b and E_c is difficult, if at all possible. Last but not least, DWSC models require a constant p_{opt}. Therefore we suggest 0·25 as an appropriate value for p_{opt}. This value will be used from here on.

While p_{opt} is fairly independent from the controlling dimensionless numbers, one must realize that actual errors are not. Indeed, the L_2-norms in tests 2–5 show a significant dependence on Γ (Figure 5)

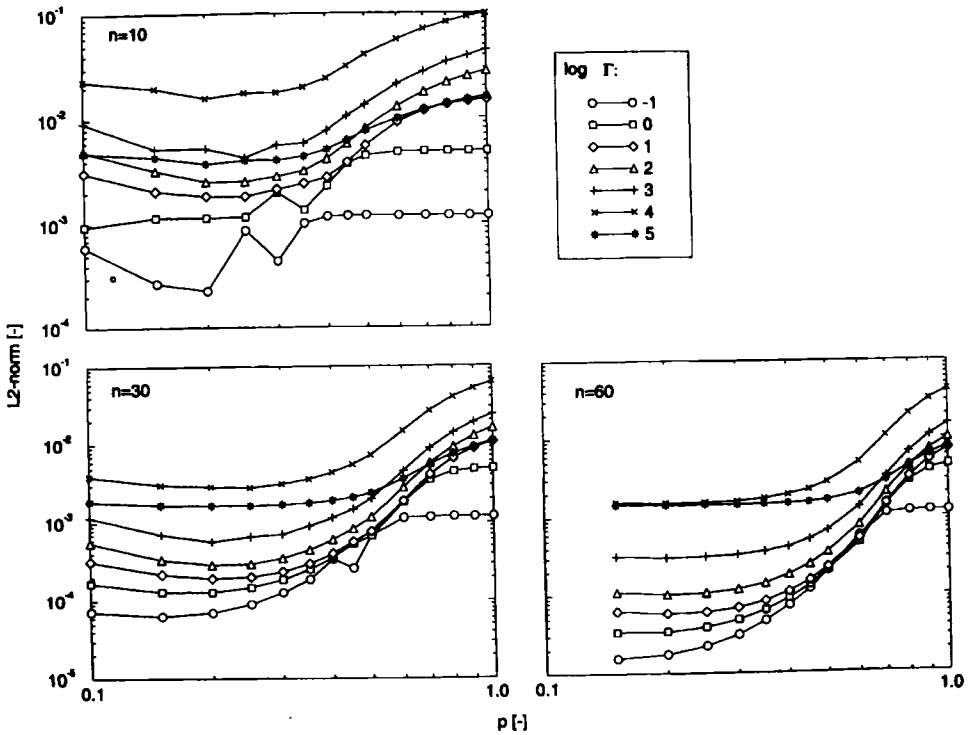

Figure 5. Test 2. Influence of Γ on p_{opt} for three different numbers n of nodes

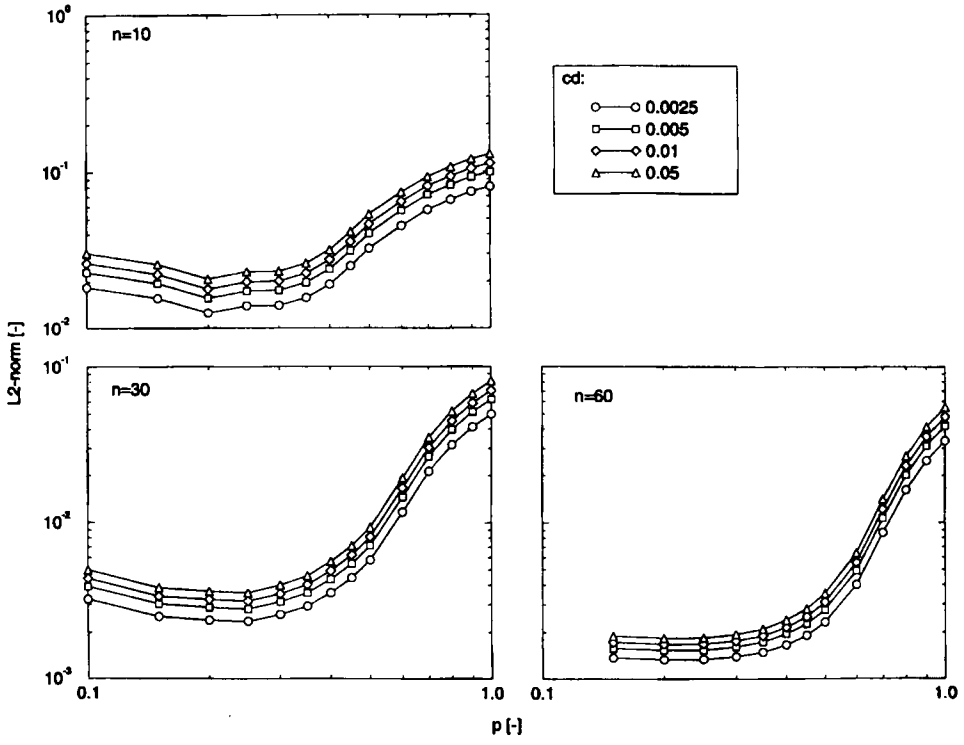

Figure 6. Test 3. Influence of c_d on p_{opt} for three different numbers n of nodes

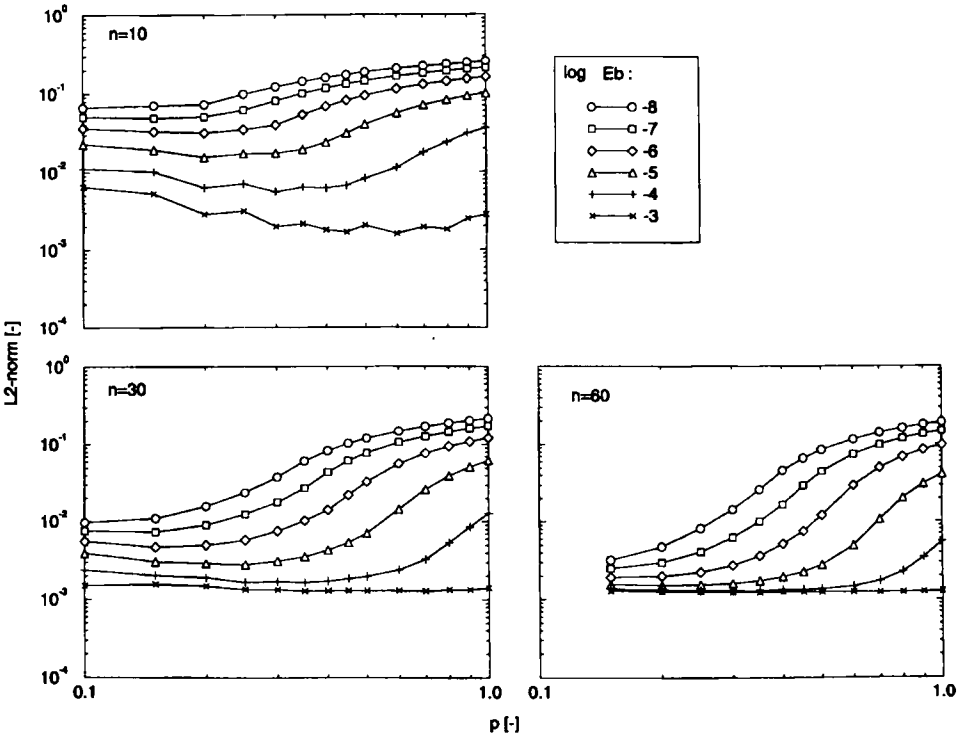

Figure 7. Test 4. Influence of E_b on p_{opt} for three different numbers n of nodes

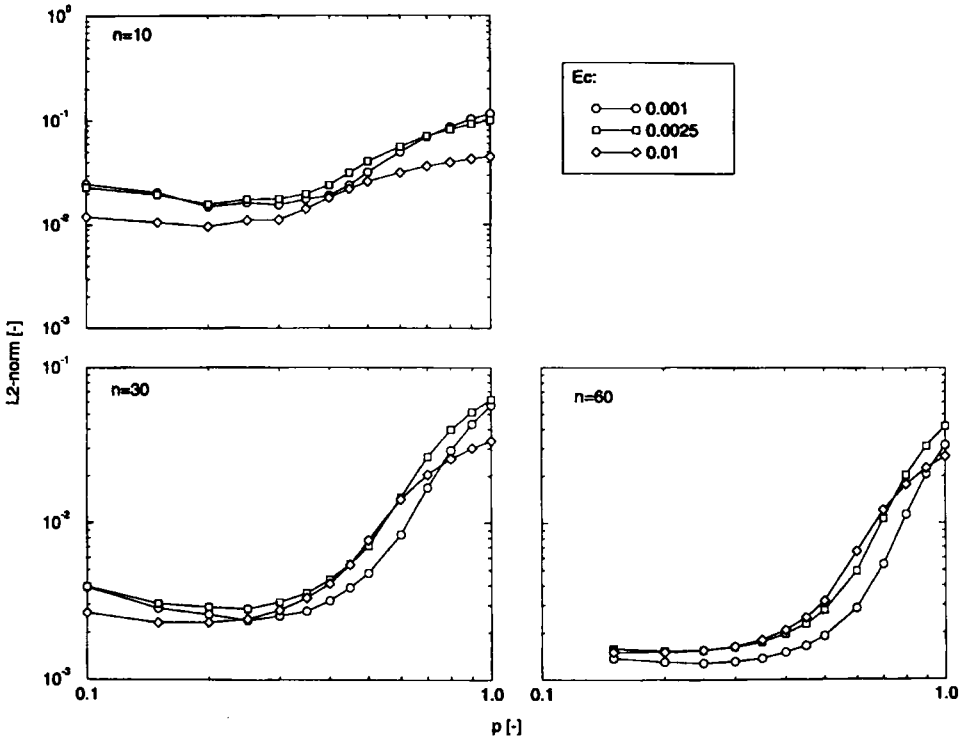

Figure 8. Test 5. Influence of E_c on p_{opt} for three different numbers n of nodes

and, to a lesser extent, on E_b (Figure 7); only the dependence on c_d (Figure 6) and E_c (Figure 8) is weak.

3.4. *Verification*

In test 6 we repeat a 1D experiment reported by Davies.[21] Our purpose is twofold. First, the optimized β grid ($p = 0{\cdot}25$) is compared against previously available grids. Secondly, its performance is assessed for conditions different from the ones for which it was derived. Namely, a no-slip condition is used at the bottom and the eddy viscosity varies in time:

$$A_v = 0{\cdot}2\frac{e(\sigma)}{\bar{e}}\bar{u}^2, \qquad e(\sigma) = \begin{cases} e_b + (1+\sigma)(e_c - e_b)/0{\cdot}2, & -1 \leqslant \sigma \leqslant -0{\cdot}8, \\ e_b, & -0{\cdot}8 \leqslant \sigma \leqslant 0, \end{cases} \tag{16}$$

where $(e_b, e_c, \bar{e}) = (0{\cdot}0001, 0{\cdot}1, 0{\cdot}09001)$ and $\bar{u}$ is the depth-averaged velocity. The freestream velocity is 1 m s^{-1} and the wave period 12 h (S_2 tide).

Velocity amplitudes and phases at selected points in the vertical were compared with results from the reference grid (Table II). Grid β with 30 nodes and the logarithmic and log–linear grids with 60 nodes have a similar accuracy. For the same number of nodes the results from grid β are clearly better than those from both the logarithmic and log–linear grids. Grid β therefore represents an improvement over other available discretization approaches.

Results also suggest that β grids and the optimization criterion derived in the previous section are robust (or at least lead to accurate numerical solutions) beyond the original conditions of friction

Table II. Test 6. Results from reference grid and differences between results from various test grids and reference grid. Velocity amplitudes are in metres per second; phases (in parentheses) are in degrees. Results for logarithmic and log–linear grids are from Reference 21

Sigma	Reference (10^4 nodes)	Log–linear (60 nodes)	Logarithmic (60 nodes)	β (10 nodes)	β (30 nodes)	β (60 nodes)
			S_2, $h=10$ m			
−0·995	0·215 (211)	−0·019 (−2)	0·008 (0)	−0·040 (−2)	−0·007 (−1)	−0·004 (0)
−0·99	0·259 (211)	−0·018 (−2)	0·009 (0)	−0·038 (−2)	−0·007 (0)	−0·004 (0)
−0·9	0·402 (213)	−0·012 (−1)	0·015 (0)	−0·030 (−2)	−0·009 (0)	−0·006 (0)
−0·75	0·453 (214)	−0·010 (−1)	0·016 (0)	−0·029 (−2)	−0·009 (0)	−0·007 (0)
−0·5	0·502 (215)	−0·008 (−1)	0·015 (0)	−0·026 (−1)	−0·009 (0)	−0·008 (0)
			S_6, $h=10$ m			
−0·995	0·026 (121)	−0·002 (−8)	0·000 (0)	−0·003 (−11)	0·000 (−3)	−0·001 (−2)
−0·99	0·031 (124)	−0·001 (−8)	0·001 (0)	−0·002 (−10)	0·001 (−3)	0·001 (−2)
−0·9	0·049 (136)	0·001 (−7)	0·002 (0)	−0·001 (−8)	0·000 (−2)	0·000 (−1)
−0·75	0·055 (143)	0·003 (−7)	0·004 (−1)	−0·001 (−7)	0·001 (−3)	0·001 (−2)
−0·5	0·062 (150)	0·004 (−8)	0·005 (−2)	0·000 (−6)	0·000 (−2)	0·000 (−2)
			S_2, $h=100$ m			
−0·995	0·554 (244)	−0·007 (−1)	−0·011 (0)	−0·065 (−4)	−0·008 (0)	−0·002 (0)
−0·99	0·654 (246)	−0·006 (0)	−0·011 (0)	−0·048 (−3)	−0·005 (0)	−0·001 (0)
−0·9	0·928 (256)	−0·003 (0)	−0·005 (1)	−0·013 (−1)	−0·004 (0)	−0·002 (1)
−0·75	0·991 (261)	−0·002 (0)	−0·002 (1)	−0·009 (−1)	−0·003 (0)	−0·002 (0)
−0·5	1·023 (267)	−0·002 (−1)	−0·001 (0)	−0·004 (−1)	−0·003 (−1)	−0·003 (0)
			S_6, $h=100$ m			
−0·995	0·070 (218)	0·001 (0)	0·000 (−9)	0·003 (−4)	0·001 (0)	0·001 (1)
−0·99	0·069 (226)	0·001 (−1)	−0·001 (−8)	0·004 (−3)	0·001 (0)	0·001 (1)
−0·9	0·036 (278)	0·000 (−1)	−0·003 (−6)	0·005 (−2)	0·000 (1)	−0·001 (1)
−0·75	0·023 (319)	−0·001 (0)	−0·003 (0)	0·004 (−3)	0·000 (1)	−0·001 (1)
−0·5	0·013 (13)	0·001 (5)	0·000 (32)	0·004 (1)	0·001 (3)	0·000 (3)

parametrization. Experiments were repeated with $p=0{\cdot}2$ and $0{\cdot}3$. The results were very similar, further suggesting that $0{\cdot}25$ is an appropriate value for p_{opt} even for time-dependent eddy viscosity profiles.

4. HORIZONTAL NODAL DISTRIBUTION

We now address the issue of distributing among verticals the total number of nodes available for the domain. Within DWSC formulations this problem is non-existent as all verticals must have the same number of nodes. However, LSC formulations allow more nodes to be placed in the verticals where finer resolution is necessary for accuracy reasons.

We have shown earlier that $L_2(v)$ depends very significantly on Γ and less significantly on the other controlling dimensionless numbers. Γ is also fairly straightforward to evaluate. It is therefore both reasonable and convenient to argue that criteria to guide the distribution of the number of nodes among verticals should account for the spatial distribution of Γ. The difficulty is to define a relationship between n and Γ that leads to optimal accuracy within a chosen constraint (e.g. a certain total number of nodes in the entire domain or a certain maximum error).

A possible approach, which we will explore below, is to assume that errors are exclusively a function of n and Γ and look for a distribution of nodes that keeps errors constant with regard to these two

parameters, i.e.

$$\mathrm{d}\log\Theta = \left(\frac{\partial}{\partial \log \Gamma}\mathrm{d}\log\Theta\right)\mathrm{d}\log\Gamma + \left(\frac{\partial}{\partial \log n}\mathrm{d}\log\Theta\right)\mathrm{d}\log n, \tag{17}$$

where Θ denotes an error measure. Only error measures that display the functional dependence identified above for $L_2(v)$ should be retained. An example that will be used in the next section is

$$L_2(u) = UL_2(v) = \frac{\Gamma h}{T} L_2(v). \tag{18}$$

From (17) we can now derive the desired relationship between n and Γ as

$$\frac{\mathrm{d}\log n}{\mathrm{d}\log\Gamma} = -\frac{\dfrac{\partial}{\partial \log \Gamma}\log\Theta}{\dfrac{\partial}{\partial \log n}\log\Theta}. \tag{19}$$

For this relationship to be of any practical significance, however, we need to be able to quantify the right-hand side (RHS). This is non-trivial. While it can be argued that $\mathrm{d}\log\Theta/\mathrm{d}\log n$ is approximately a constant (e.g. see Figure 9 for $\Theta = L_2(v)$ linked to the order of accuracy of the numerical solution method, the behaviour of $\mathrm{d}\log\Theta/\mathrm{d}\log\Gamma$ is unknown *a priori*, is likely very sensitive to the choice of Θ and may be impossible to characterize even experimentally.

It is, however, reasonable to assume a functional form for the RHS of (19) based on 'best available information', construct the grid and evaluate errors *a posteriori* to assess how well (17) is observed. We will experiment with this concept in the next section, making the simple assumption that the RHS is a constant (based on Figure 9 for $\Theta = L_2(v)$) and rewriting (19) as

$$n = n_{\min}\left(\frac{n_{\max}}{n_{\min}}\right)\log(\Gamma/\Gamma_{\min})/\log(\Gamma_{\max}/\Gamma_{\min}), \tag{20}$$

where $n_{\min}$ and $n_{\max}$ are user-specified maximum and minimum numbers of nodes per vertical and $\Gamma_{\max}$ and $\Gamma_{\min}$ are maximum and minimum values of Γ in the domain. The choice of $n_{\min}$ and $n_{\max}$ dictates the value of $\mathrm{d}\log\Theta/\mathrm{d}\log\Gamma$, which is convenient from the user viewpoint but does not necessarily represent the true behaviour of this term.

The use of (20) requires that Γ, which is not known *a priori*, be estimated. Three levels of decreasing complexity are considered here for the estimation of Γ, all based on the combination of (5) and (8). If the amplitudes and phases of the main tidal constituent are known (e.g. from a depth-

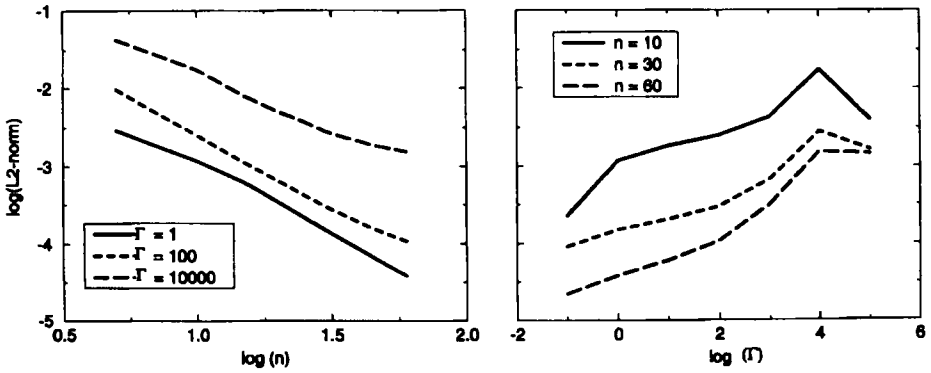

Figure 9. Variation in $L_2(v_A)$ with n and Γ. Default values of c_d, E_b and E_c were used (Table I)

averaged simulation), Γ can be evaluated as (level 3)

$$\Gamma = \frac{gT^2}{2\pi h}\sqrt{[(\nabla A)^2 + (A\nabla\phi)^2]}. \tag{21}$$

The gradient operator is used here because we are interested in the maximum value of Γ in each vertical.

A simpler alternative (level 2), which does not require a preliminary run, is to neglect amplitude variations in the domain and estimate Γ as

$$\Gamma \approx AT\sqrt{(g/h^3)}. \tag{22}$$

In this case, only depth effects are considered on the variation in Γ. While these effects are generally dominant in deep waters, they can be secondary in estuarine conditions (e.g. relative to lateral constraints).

Finally (level 1), we can ignore the variations in Γ altogether, leading to a constant number of nodes per vertical. This level is the only one that can be applied with DWSC models.

The performance of each level is illustrated in the next section.

5. APPLICATION

The criteria and concepts developed in Sections 3 and 4 are now applied in the context of a synthetic but relatively complex estuary. Our primary objective is to evaluate whether the overall approach is useful beyond the very narrow limits of the adopted simplifying assumptions. For this purpose we choose a case where the rigid lid approximation does not apply, we use a time-dependent eddy viscosity and we solve both the internal and external modes.

The application consists of a tidal wave propagating from deep into shallow waters. The domain (Figure 10) schematically represents a shallow embayment connected by a narrow mouth to a continental shelf and continental slope. A two-dimensional, laterally averaged model, RITA_{2v}[26] is used to make Γ vary owing to both topographic and geometric effects. RITA_{2v} solves the external mode with the generalized wave continuity equation[27] using linear finite elements. The internal mode equations are discretized as described in Section 2.

A time-dependent eddy viscosity parametrization proposed by Davies and Lawrence[28] is used. In the upper 80 per cent of the water column the eddy viscosity coefficient is given by

$$A_v = K|\bar{u}|\Delta, \tag{23}$$

where $\bar{u}$ is the depth-averaged velocity, K is a dimensionless coefficient taken as 0·0025 and the depth of the bottom boundary layer, Δ, is computed as

$$\Delta = \min(h, 2000\sqrt{(|\tau_b|/\rho)}). \tag{24}$$

In the bottom 20 per cent of the water column, A_v decreases linearly to

$$A_{vb} = \max(\kappa z_0\sqrt{(|\tau_b|/\rho)}, \mu), \tag{25}$$

where μ is the molecular viscosity of water (10^{-6} m^2 s^{-1}). The friction coefficient c_d is set to 0·01.

Four grids were built (Figure 11), all using the same horizontal nodal spacing ($\Delta x = 1000$ m) but each having a different vertical discretization: G0 is uniform, while G1–G3 are β grids and correspond respectively to levels 1–3 of the criterion discussed in the previous section. The total number of nodes is roughly the same for all grids, but their distribution varies: G0 and G1 have 10 nodes per vertical, while in G2 and G3 n varies according to (20), with Γ computed with (22) and (21) respectively (Figure 12). For the last two grids we set $n_{min} = 5$, which leads to $n_{max} = 15$ for G2 and $n_{max} = 24$ for

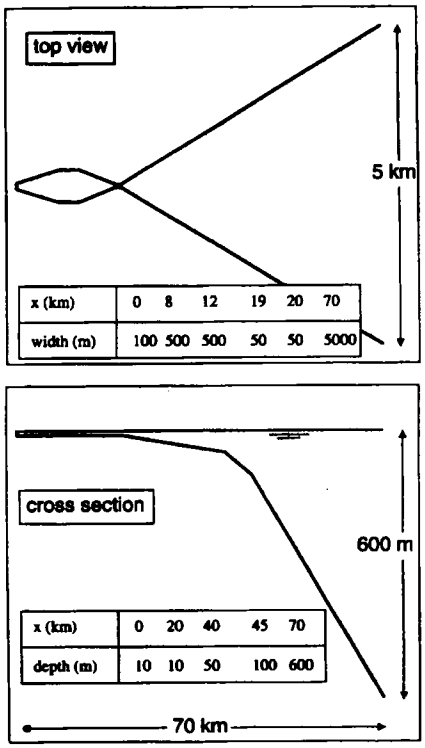

Figure 10. Domain for synthetic application

G3. To build G3, a preliminary depth- averaged simulation was performed for a single constituent (S_2) and the resulting amplitudes and phases were used to evaluate Γ (Figure 13).

The comparison between the four grids implicitly assumes similar costs, i.e. a CPU time for the internal mode directly related to the number of nodes. This assumption is valid since the internal mode matrices are tridiagonal, requiring only $O(n)$ operations to invert.[29]

The model is forced at the open boundary with S_2 ($T=12$ h) and S_1 ($T=24$ h) waves with amplitudes of 1 and 0·5 m respectively. All non-linear terms are included, except advective accelerations. The model is run for 10 S_1 tidal cycles in depth-averaged mode plus five cycles in 2D mode. The time step is 60 s. Results from the last cycle are harmonically analysed at regularly spaced verticals, where the L_2-norms of the velocity amplitudes, $L_2(u_A)$, are evaluated. The reference grid has the same horizontal resolution as the test grids and a β grid with 60 nodes per vertical. The time step of the reference simulation is 30 s.

Figure 14 shows $L_2(u_A)$ along the channel for representative constituents (S_0, S_1, S_2 and S_6). Results for other constituents (S_3, S_4 and S_5) display similar trends and are not shown here.

For G0, errors typically present a maximum in the channel (e.g. 0·1 m s^{-1} for S_2) and are smallest in deep water (2×10^{-5} m s^{-1} for the same constituent). The error peak should be attributed both to larger velocities and to a rapid change in the wave amplitudes and phases (Figure 13). This change in wave characteristics corresponds to a maximum in the value of Γ, which, as shown in the 1D tests, leads to the largest errors.

The use of grid G1 dramatically improves the results, with L_2-norms decreasing almost uniformly for all frequencies by a factor of 10 (Figure 14). Still, the difference between maximum and minimum

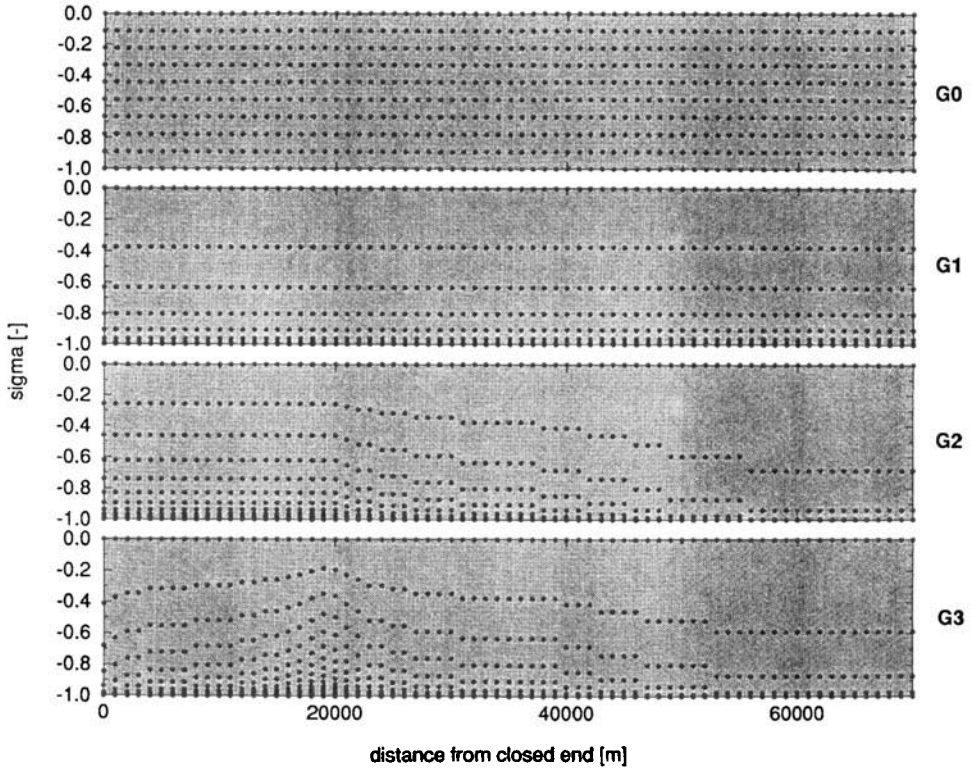

Figure 11. Grids used in application

errors persists, indicating a relative over-refinement in deep water. This difference suggests that LSCs can further improve the overall accuracy.

The errors for grid G2 decrease in the estuary and increase in the continental slope, because this grid concentrates more nodes in shallow water. As a result, the errors are more uniform than those obtained with G1. However, not enough resolution is provided in the channel, because G2 ignores geometry effects on Γ, and the already small errors observed with G1 near the closed boundary are further decreased. As discussed in the previous section, level 2 of the criterion is not well-suited for estuarine applications, because lateral constraints are not accounted for.

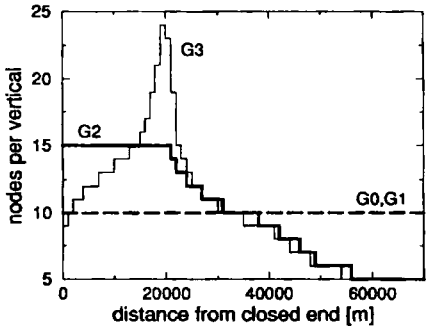

Figure 12. Number of nodes per vertical. Total numbers of nodes are 710 for G0 and G1, 711 for G2 and 703 for G3

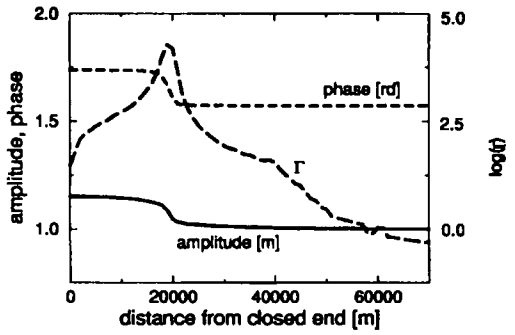

Figure 13. S_2 characteristics: Γ and elevation amplitudes and phases (1D simulation)

Grid G3 leads to the best results. Relative to G1, it typically reduces the maximum, mean and standard deviation of the L_2-norms by a factor of three to six. Inside the estuary the errors are similar to G2's, even though G2 has more modes in this area; in the channel, G3 leads to better results than G2. As a result, the L_2-norms for G3 are the smallest and the most uniform.

We note (Figure 15) that $\log L_2(u)$ varies approximately linearly with $\log \Gamma$, as assumed in our discussion of (19). However, the value of the slope inherently assumed in (20) with $n_{\min} = 5$ and $n_{\max} = 24$ is 0·13, against an observed slope of 0·61 (Figure 15). Our interpretation is that we could make $L_2(u)$ more uniform in G3 by adjusting $n_{\min}$ in order to obtain a larger imposed slope.

It is also interesting to observe the variation in $\log L_2(v)$ with $\log \Gamma$ (Figure 15). For this error measure the assumption of a linear variation breaks down. Coincidentally (results not shown), mean $L_2(v)$ results are not significantly better for grids G2 and G3 than for grid G1. Our interpretation is that

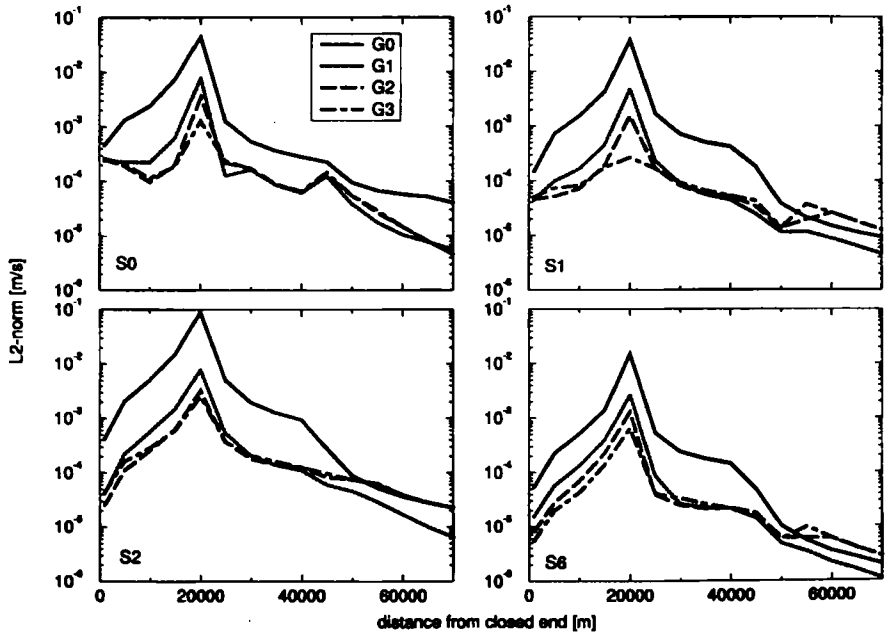

Figure 14. $L_2(u_A)$ for grids G0–G3

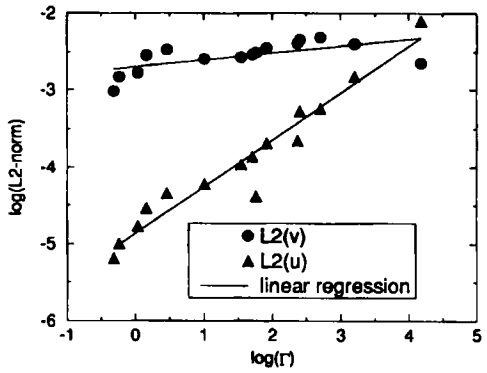

Figure 15. Linear regression for $\log L_2(v_A)$ (slope 0·09, correlation coefficient 0·62) and $\log L_2(u_A)$ (slope 0·61, correlation coefficient 0·97) versus $\log \Gamma$ for grid G1

to optimize the distribution of $L_2(v)$ in the domain, we would need to use in (20) a higher-order function to describe the dependence of $\log L_2(v)$ on $\log \Gamma$.

The choice of the error norm that we want to equalize over the domain is somewhat ambiguous and will affect the outcome. Norms based on absolute errors can lead to large erroneous fluxes in deep waters, which can be amplified in shallow waters. Norms based on relative errors can be overly stringent in deep waters, leading to errors far below the detection limits of current instruments. Our choices in this paper were pragmatic: in the 1D tests, only relative errors ($L_2(v)$) could be computed; in the 2D application, absolute errors ($L_2(u)$) led to overall best results.

6. FINAL CONSIDERATIONS

This paper addressed the vertical discretization in barotropic tidal models. Criteria for both the nodal distribution within a given vertical and the horizontal distribution of the total number of nodes were developed and showed promising results in a synthetic application.

Our analysis demonstrated the strong dependence of errors on local flow properties. An efficient vertical discretization should take those properties into account, which is not possible with either DWSCs or z-co-ordinates. Thanks to their flexibility, LSCs appear therefore to be a strong alternative to the previous methods.

The usefulness of LSCs should extend well beyond the cases explored in this paper. For instance, a method recently developed, in which the momentum equations are solved for Reynold stresses rather than velocities,[30] can also benefit highly from LSCs. Numerical experiments with a barotropic tidal model showed that the number of nodes per vertical needed to achieve a 1 per cent error in the bottom friction varied from two to 52, depending on the physical parameters.[31] Clearly, using the same number of vertical nodes throughout the domain will lead to a large errors and/or over-refinements.

The degree of refinement adequate for a given vertical was shown to depend on a dimensionless number Γ which characterizes local changes in wave properties. This number may also prove useful to derive criteria for the horizontal discretization of tidal models. Indeed, the usual criterion for horizontal discretization based on the dimensionless wavelength is inadequate in areas of rapid changes in wave properties owing to its inability to take into account the two-dimensional structure of the flow and the rate of change in wavelength.[32,33] The number Γ, based on horizontal gradients of the wave amplitude and phase, may provide a good indication as to where horizontal resolution is most needed.

This paper constitutes only a first step towards the development of solid guidelines to discretize the vertical dimension in surface water models and certainly leaves many questions unanswered. Out of necessity, several simplifying assumptions were made that may eventually have to be revisited. Important open questions include

(i) the dependence of p_{opt} on the chosen turbulence closure scheme
(ii) the extension of the proposed criteria to other types of vertical grids
(iii) the validity of the proposed criteria in 3D barotropic flows
(iv) the implications of stratification on the choice of grid type and on the development of optimization criteria.

ACKNOWLEDGEMENTS

We thank Ms. Anabela Oliveira for useful discussions. The first author was sponsored by Junta Nacional de Investigação Científica e Tecnológica (Portugal) under grant BD-1786/91-IG and the second author was partially sponsored by NSF grant OCE-9412028.

REFERENCES

1. J. J. Leendertse and S. K. Liu, 'A three-dimensional model for estuaries and coastal seas. II. Aspects of computation', *Rand Corporation Rep. R-1764-OWRT*, 1975.
2. V. Casulli and R. T. Cheng, 'Semi-implicit finite difference methods for three-dimensional shallow water flow', *Int. j. numer. methods fluids*, **15**, 629–648 (1992).
3. A. F. Blumberg and G. L. Mellor, 'A description of a three- dimensional coastal ocean circulation model', in N. S. Heaps (ed.), *Three-Dimensional Coastal Ocean Models*, CES Vol. 4, AGU, Washington, DC, 1987, pp. 1–16.
4. D. R. Lynch and F. E. Werner, 'Three-dimensional hydrodynamics on finite elements. Part II: Non-linear time-stepping model', *Int. j. numer. methods fluids*, **12**, 507–533 (1991).
5. R. A. Walters, 'A 3D, finite element model for coastal and estuarine circulation', *Continental Shelf Res.*, **12**, 83–102 (1992).
6. R. T. Cheng and P. E. Smith, 'A survey of three-dimensional numerical estuarine models', *Proc. Conf. on Estuarine and Coastal Modeling*, ASCE, New York, 1990, pp. 1–15.
7. J. M. Gary, 'Estimate of truncation error in transformed coordinate, primitive equation atmospheric models', *J. Atmos. Sci.*, **30**, 223–233 (1973).
8. R. L. Haney, 'On the pressure gradient force over steep topography in sigma coordinate ocean models', *J. Phys. Oceanogr.*, **21**, 610– 619 (1991).
9. E. Deleersnijder and J. M. Beckers, 'On the use of the σ- coordinate system in regions of large bathymetric variation', *J. Marine Syst.*, **3**, 381–390 (1992).
10. R. P. Signell, H. L. Jenter and A. F. Blumberg, 'Modeling the Seasonal Circulation in Massachussets Bay', *Proc. 3rd Int. Conf. on Estuarine and Coastal Modeling*, ASCE, New York, 1994, pp. 578–590.
11. J. D. McCalpin, 'A comparison of second-order and fourth-order pressure gradient algorithms in a σ-coordinate ocean model', *Int. j. numer. methods fluids*, **18**, 361–383 (1994).
12. G. S. Stelling and J. A. Th. M. van Kester, 'On the approximation of horizontal gradients in sigma coordinates for bathymetry with steep bottom slopes', *Int. j. numer. methods fluids*, **18**, 915–935 (1994).
13. A. B. Fortunato and A. M. Baptista, 'Modeling near-bottom advective acceleration in surface water models', *Proc. Int. Conf. on Computational Methods in Water Resources X*, Kluwer, Dordrecht, 1994, pp. 1045–1052.
14. A. B. Fortunato and A. M. Baptista, 'Localized sigma coordinates for the vertical structure of hydrodynamic models', *Proc. 3rd Int. Conf. on Estuarine and Coastal Modeling*, ASCE, New York, 1994, pp. 323–335.
15. J. P. Laible, 'On the solution of the three-dimensional shallow water equations using the wave equation formulation', *Proc. Int. Conf. on Computational Methods in Water Resources IX*, Computational Mechanics Publications, Southampton, 1992, pp. 545–552.
16. A. B. Fortunato and A. M. Baptista, 'A comparison of two methods to evaluate horizontal gradients in surface water models', *Atmos. Ocean*, 1996, in press.
17. A. M. Davies, 'Numerical problems in simulating tidal flows with a frictional-velocity-dependent eddy viscosity and the influence of stratification', *Int. j. numer. methods fluids*, **16**, 105–131 (1993).
18. J. J. Westerink, R. A. Luettich Jr. and J. C. Muccino, 'Modeling tides in the western North Atlantic using unstructured graded grids', *Tellus*, **46A**, 178–199 (1994).
19. B. J. Noye, 'Finite difference techniques for partial differential equations', in B. J. Noye (ed.), *Computational Techniques for Differential Equations*, North-Holland, Amsterdam, 1984, pp. 95–354.

20. B. J. Noye and M. Stevens, 'A three-dimensional model of tidal propagation using transformations and variable grids', in N. S. Heaps (ed.), *Three-Dimensional Coastal Ocean Models*, CES Vol. 4, AGU, Washington, DC, 1987, pp. 41–69.
21. A. M. Davies, 'On the accuracy of finite difference and modal methods for computing tidal and wind waves current profiles', *Int. j. numer. methods fluids*, **12**, 101–124 (1991).
22. K. W. Bowden and S. R. Ferguson, 'Variations with height of the turbulence in a tidally induced bottom boundary layer', in J. C. J. Nihoul (ed.), *Marine Turbulence, Proc. 11th Liege Colloq. on Ocean Hydrodynamics*, EOS Vol. 28, Elsevier, Amsterdam, 1980, pp. 259–286.
23. A. M. Davies, 'A bottom boundary layer resolving three-dimensional tidal model: a sensitivity study of eddy viscosity formulation', *J. Phys. Oceanogr.*, **23**, 1437–1453 (1993).
24. A. M. Davies and J. Aldridge, 'A numerical model study of parameters influencing tidal currents in the Irish Sea', *J. Geophys. Res.*, **98**, 7049–7067 (1993).
25. A. M. Davies, 'On the importance of time varying eddy viscosity in generating higher tidal harmonics', *J. Geophys. Res.*, **95**, 20,287–20,312 (1990).
26. A. B. Fortunato and A. M. Baptista, 'RITA$_{2v}$ user's manual. 2D vertical hydrodynamic model for river and tidal analysis. Part I—Flow model', *OGI-CCALMR Software Documentation Series SDS7, 93- 3*, Oregon Graduate Institute, Portland, OR, 1993.
27. I. P. E. Kinmark, 'The shallow water equations: formulation, analysis and application', in C. A. Brebia and S. A. Orszag (eds), *Lecture Notes in Engineering*, Vol. 15, Springer, Berlin, 1985.
28. A. M. Davies and J. Lawrence, 'Modelling the non-linear interaction of wind and tide: its influence on current profiles', *Int. j. numer. methods fluids*, **18**, 163–188 (1994).
29. W. H. Press, S. A. Teukolsky, W. T. Vetterling and B. P. Flannery, *Numerical Recipes in C*, Cambridge University Press, Cambridge, 1988.
30. R. A. Luettich Jr. and J. J. Westerink, 'A solution for the vertical variation of stress, rather than velocity, in a three-dimensional circulation model', *Int. j. numer. methods fluids*, **12**, 911–928 (1991).
31. R. A. Luettich Jr., S. Hu and J. J. Westerink, 'Development of the direct stress solution technique for three-dimensional hydrodynamic models using finite elements', *Int. j. numer. methods fluids*, *19*, 295–319 (1994).
32. J. J. Westerink, J. C. Muccino and R. A. Luettich Jr., 'Resolution requirements for a tidal model of the western North Atlantic and the Gulf of Mexico', *Proc. Int. Conf. on Computational Methods in Water Resources IX*, Elsevier, Amsterdam, 1992, pp. 667–674.
33. J. J. Westerink, R. A. Luettich Jr. and S. C. Hagen, 'Meshing requirements for large scale coastal ocean tidal models', *Proc. Int. Conf. on Computational Methods in Water Resources X*, Kluwer, Dordrecht, 1994, pp. 1323–1330.